Proceedings of the International Symposium on Physics of Materials (ISPMA13)

In Situ Investigation of Microstructure Evolution during Solidification of Mg10CaxGd (x = 5, 10, 20) Alloys

C.L. Mendis[a,*], D. Tolnai[a], A. Stark[b], N. Schell[c], K.U. Kainer[a] and N. Hort[a]

[a]Magnesium Innovation Centre, Helmholtz-Zentrum Geesthacht, Max Planck Str. 1, Geesthacht D-21502, Germany
[b]Department of Metal Physics, Helmholtz-Zentrum Geesthacht, Max Planck Str. 1, Geesthacht D-21502, Germany
[c]Structural Research on New Materials, Helmholtz-Zentrum Geesthacht, Outstation at DESY, Notkestr. 85, Hamburg D–22761, Germany

Mg–Ca–Gd based alloys are investigated as a potential alloy for degradable biomaterials with some promising results. In this investigation the Mg10CaxGd (x = 5, 10, 20) were investigated with synchrotron radiation X-ray diffraction during solidification to follow the phase evolution at two different cooling rates at 5 and 50 K min^{-1}. All three alloys show formation of α-Mg followed by Mg_2Ca phase, while only Mg10Ca20Gd alloy contained Mg_5Gd phase during solidification. During cooling α-Mg was first observed between 628 and 632 °C at a cooling rate of 5 K min^{-1} while this decreased to 620–628 °C with the increase in cooling rate to 50 K min^{-1}. The change in cooling rate from 5 to 50 K min^{-1} did not change the types of intermetallic phases observed but resulted in suppressing temperatures at which the intermetallic phases were first detected.

DOI: 10.12693/APhysPolA.128.606
PACS: 81.05.Bx, 81.30.Fb

1. Introduction

Magnesium alloys have attracted significant interest in the last two decades due to their relatively low density compared with other structural alloys in applications where light weight is of importance. Recently the interest in magnesium alloys extends to include degradable biological implants due to their biocompatibility and degradation in biological environments. Mg–RE (RE = rare earth) based, especially Mg–Gd based [1], alloys have shown to form the basis of a class of high strength and creep resistant alloys that have been developed to be used in structural settings where elevated temperature stability is of importance as well as high strength at room temperatures. Mg–Gd [1] and Mg–Gd–Dy [2] alloys are also studied extensively due to the low degradation rates observed in *in vitro* investigations for degradable biological implants.

A large amount of RE additions is required for appreciable strengthening increments through either formation of intermetallic particles along the grain boundaries or through formation of a high density of precipitates during isothermal ageing heat treatments. For Mg–Gd alloys a minimum of 10 wt% of Gd is required for appreciable increment in strengths through precipitation hardening [1]. More than 15 wt% Gd is required to form intermetallic particles along the grain boundaries to provide strengthening due to the presence of intermetallic particles in the cast alloys [1]. The high content of Gd required and the prohibitive cost of RE additions results in Mg–Gd alloys not attractive for all but specialist structural applications. Thus, there is continued interest in developing alloys that retain the attractive properties of Mg–(10–20)Gd alloys but with significantly lower Gd contents. The addition of Zn [3] and Al [4] to the Mg–Gd system has shown to produce a high density of long period stacking ordered (LPSO) phases with relatively lower concentrations of Gd while retaining higher strengths. It has been also shown that the addition of Zn to alloys containing relatively lower concentrations (≈6 wt%) Gd show remarkable increments in precipitation hardening [5]. Similar observations are made with the addition of silver to Mg–6Gd alloy [6].

Ca has been shown to behave in a manner similar to Gd in magnesium alloys with similar modifications to the texture of magnesium alloys [7]. However, Ca has a much lower solid solubility in magnesium and forms intermetallic particles along the grain boundaries [8]. The effect of Ca addition to Mg–Gd alloys on the microstructural evolution during casting has not been investigated. Fei et al. [9] investigated a range of alloys using X-ray diffraction (XRD) electron probe micro analysis (EPMA) and scanning electron microscopy (SEM) to determine the magnesium rich end of the ternary phase diagram at 400 °C. In this study a ternary phase with a crystal structure and lattice parameters similar to $Mg_{41}Ce_5$ [9] phase, denoted T phase, was detected using XRD and SEM. However, the exact nature of this ternary phase is yet to be elucidated, He et al. [10] investigating the effect of 0.4–0.6 wt% Ca addition to a Mg10Gd3Y0.4Zr (wt%) found that new cuboidal type precipitates were found at grain boundaries containing Gd, Y and Ca. In Mg3.8Zn2.2Ca (wt%) alloys addition of Gd did not affect the microstructure, especially the solid-state precipitation, during heat treatments, but had a slight influence on the mechanical properties.

*corresponding author; e-mail: Chamini.mendis@hzg.de

The work to date shows that the addition of Ca to Mg–Gd alloys may result in improving mechanical properties and strengthening through modifying intermetallic particles that form during solidification. However, there is a lack of information on changing the ratio between Ca and Gd on the microstructure evolution during solidification. In this contribution we report the findings from an *in situ* synchrotron radiation diffraction solidification experiment coupled with electron microscopy on the microstructure evolution in Mg–Ca–Gd alloys. The change in the Ca:Gd ratio and the cooling rates will provide information valuable for the development of phase diagrams as well as contribute to the design of Mg–Ca–Gd based alloys.

2. Experimental procedure

Pure Mg (99.99% Hydro Magnesium), was melted in a mild steel crucible and Mg-23Gd master alloy (from State Key Laboratory of Rare Earth Resource Utilization, Changchun Institute of Applied Chemistry, Chinese Academy of Sciences) and pure Ca (99% Alfa Aesar) was added to the melt at 720 °C. The melt was held at about 750 °C for 15 min to incorporate the alloying additions uniformly through the melt and stirred. The alloys were then cast into a hardened steel finger mould held at 350 °C. The chemical composition of the samples was analysed and both the nominal and the actual composition values are listed in Table I. All compositions are in wt%.

TABLE I

Actual compositions of the alloys investigated.

Alloy	Actual composition [wt%]		
	Ca	Gd	Mg
Mg10Ca5Gd	8	5	bal
Mg10Ca10Gd	8	9.5	bal
Mg10Ca20Gd	8	21	bal

The metallographic samples were prepared by grinding samples with SiC paper to 2500 grit finish and then polishing in 3 μm diamond suspension and a mixture of 1 μm diamond and OPS suspension. Scanning electron microscopy, in backscattered electron (SEM-BSE) mode, investigations were conducted with a TESCAN SEM equipped with an EDAX energy dispersive X-ray (EDX) spectrometer. The phase evolution expected for each of these alloys and the temperatures at which the expected phases will appear are calculated with Pandat Thermodynamic software and PanMg 8 database using the Scheil solidification model.

The synchrotron radiation diffraction experiments during solidification of the alloys were conducted at the PETRA III P07 High Energy Materials Science (HEMS) Beamline of Helmholtz Zentrum Geesthacht (HZG) at the Deutsches Elektronen-Synchroton (DESY). The measurements were performed in the chamber of a Bähr 805 dilatometer in Ar flow. The beam energy used in this investigation was set at 100 keV which corresponds to a wavelength of 0.0124 nm. The dilatometer has been modified for *in situ* synchrotron radiation measurements, there are two windows on the sides covered by Kapton foil, which is transparent for the X-ray beam, and the induction coil opened in the middle so that the beam passes through only the sample and the crucible. During the test the sample was contained in graphite crucibles closed with titanium lids with a type S thermocouple controlling the measurement welded onto the surface of the lid. Samples of the investigated alloys were heated to 750 °C at 40 K min^{-1} held at 750 °C for 10 min. The samples were then cooled at 5 K min^{-1} or 50 K min^{-1} to 200 °C and then air cooled to follow the microstructure evolution during cooling from the melt. The 2D diffraction patterns were recorded with an acquisition time of 3.5 s ($\approx$1 K) with a Perkin Elmer XRD 1621 Flat Panel detector with a pixel size of 200×200 μm^2 and were azimuthally integrated to obtain X-ray line profiles. The information on the intermetallic phases were obtained from the Pearson Crystal Structure Database [11], the d-spacing and 2θ angles were calculated using CaRIn Crystallography 3.1™ software.

3. Results

The Scheil solidification calculations showing calculated transformation temperatures and phases expected and their volume fractions are shown in Table II. The addition of Gd to Mg10Ca alloy changes only the volume fraction of the expected phases, the types of phases observed did not change. The volume fraction of intermetallic phases also increased with Gd content with both Mg_2Ca contents reaching a maximum at Mg10Ca20Gd alloy where the main phase observed is Mg_2Ca.

TABLE II

Transformation temperatures of α-Mg and intermetallic phases predicted by the Scheil solidification calculations using Pandat 8 software.

Alloy	Temperature at which the phase is detected [°C]		
	$\alpha-$Mg	Mg2Ca	Mg5Gd
Mg10Ca5Gd	564	513	509
Mg10Ca10Gd	547	510	509
Mg10Ca20Gd	541	513	509

TABLE III

Pertinent temperatures for phase evolution observed during solidification studies using *in situ* HEXRD.

Alloy	Transformation temperatures for various phases at a given cooling rate [°C]					
	5 K min^{-1}			50 K min^{-1}		
	$\alpha-$Mg	Mg_2Ca	Mg_5Gd	$\alpha-$Mg	Mg_2Ca	Mg_5Gd
Mg10Ca5Gd	632	504	–	628	450	–
Mg10Ca10Gd	625	506	–	620	498	-
Mg10Ca20Gd	626	515	504	620	446	417

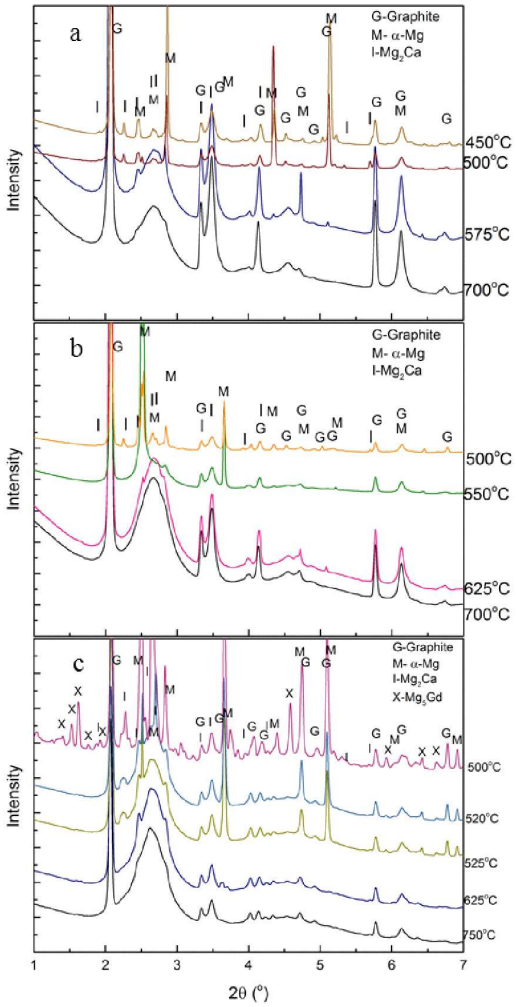

Fig. 1. *In situ* HEXRD line profiles recorded from (a) Mg10Ca5Gd (b) Mg10Ca10Gd and (c) Mg10Ca20Gd alloys during solidification at a cooling rate of 5 K min^{-1}.

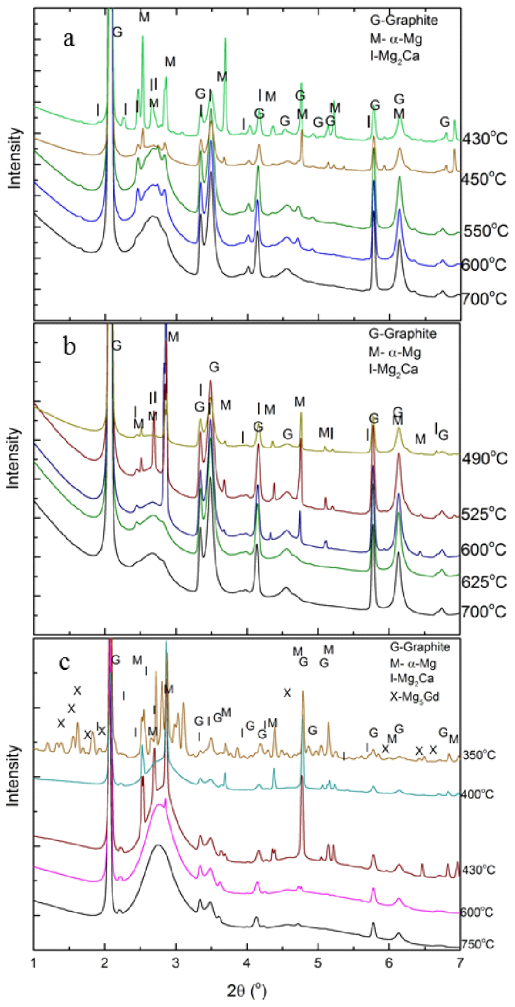

Fig. 2. As in Fig. 1, but for cooking rate of 50 K min−1.

The azimuthally integrated high energy X-ray diffraction (HEXRD) line profiles for the Mg10CaxGd ($x = 5$, 10, 20) alloys cooled at 5 K min^{-1} are shown in Fig. 1 and the temperatures at which the phase transformations occur are summarised in Table III. The first phase to solidify in all alloys was α-Mg followed by Mg_2Ca. Mg_5Gd phase was only detected in the Mg10Ca20Gd alloy using HEXRD. The α-Mg started to solidify at 632 ± 5, 625 ± 5, and 627 ± 5 °C for Mg10Ca5Gd, Mg10Ca10Gd, and Mg10Ca20Gd alloys, respectively. The Mg_2Ca phase was detected at 504 ± 5, 506 ± 5, and 515 ± 5 °C for Mg10Ca5Gd, Mg10Ca10Gd, and Mg10Ca20Gd, respectively, while Mg_5Gd was detected at 509 °C in Mg10Ca20Gd alloy.

The increase in the cooling rate to 50 K min^{-1} did not change the types of intermetallic particles observed in the HEXRD patterns, Fig. 2, and the pertinent transformation temperatures for the phases observed are summarised in Table III. However, the temperatures at which various intermetallic phases formed decreased significantly. The α-Mg was first detected at 628 ± 5, 620 ± 5, and 620 ± 5 °C for Mg10Ca5Gd, Mg10Ca10Gd, and Mg10Ca20Gd alloys, respectively. The Mg_2Ca phase was detected at 450 ± 5, 498 ± 5, and 446 ± 5 °C for Mg10Ca5Gd, Mg10Ca10Gd, and Mg10Ca20Gd, respectively, while Mg_5Gd was detected at 417 °C in Mg10Ca20Gd alloy.

The samples used for *in situ* investigation of solidification were examined with SEM to observe the solidified microstructures at both cooling rates, Fig. 3. The microstructures of samples solidified at a cooling rate of 5 K min^{-1}, Fig. 3a–c, showed that there is an increase in the amount of intermetallic phases with the increase in Gd concentration. Mg10Ca5Gd, Fig. 3a, and Mg10Ca10Gd, Fig. 3b, show backscattered electron contrast due to only one intermetallic phase whereas in Mg10Ca20Gd alloy 2 phases could be observed, Fig. 3c. The increase in the cooling rate to 50 K min^{-1} did not show any changes in the contrast due to formation of any new phases, Fig. 3d–f. However, coarsening of the microstructures, especially the intermetallic particles in the

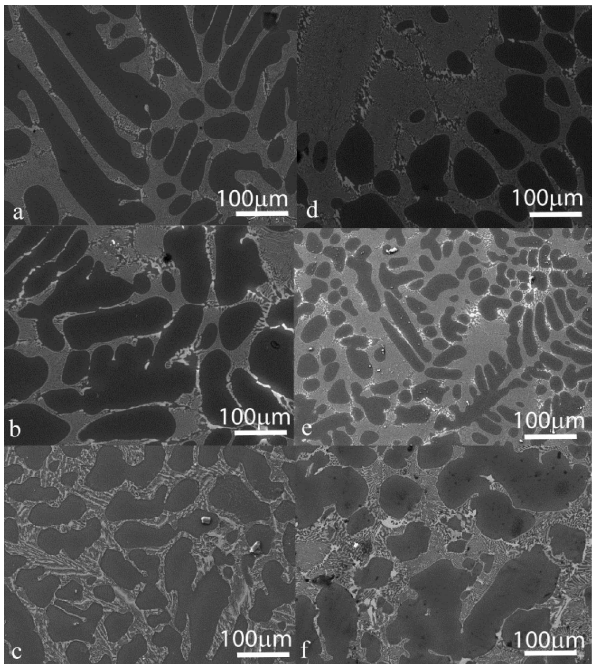

Fig. 3. SEM micrographs showing the final microstructures of the solidified samples with a cooling rate of (a–c) 5 K min^{-1} and (d–f) 50 K min^{-1} for (a, d) Mg10Ca5Gd (b, e) Mg10Ca10Gd and (c, f) Mg10Ca20Gd alloys.

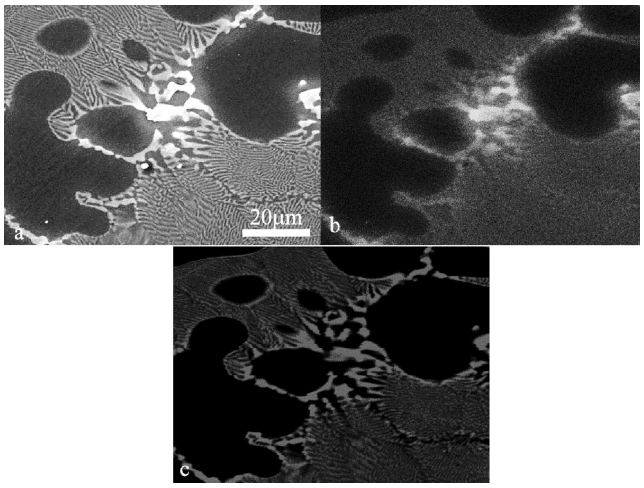

Fig. 4. EDX elemental maps recorded from Mg10Ca10Gd alloy following the *in situ* investigation during solidification at a cooling rate of 50 K min^{-1} (a) SEM image (b) Gd map and (c) Ca map.

inter-dendritic regions are observed. The Mg10Ca5Gd and Mg10Ca10Gd alloys only contained a single intermetallic phase while the increase in Gd content to 20 wt% shows the presence of two different intermetallic phases through the microstructure, Fig. 3f.

SEM EDX elemental maps for Mg10Ca10Gd cooled at 50 K min^{-1} are shown in Fig. 4 as typical of those recorded from intermetallic phases. The elemental maps show that there is Ca and Gd found in the intermetallic phase observed in the microstructure and that there is some Gd distributed through the magnesium matrix. However, there is no evidence of a second intermetallic phase observed along the inter-dendritic regions. The maps recorded from Mg10Ca10Gd alloys at 5 K min^{-1} and maps recorded from Mg10Ca5Gd alloys at both cooling rates are comparable with the results presented in Fig. 4.

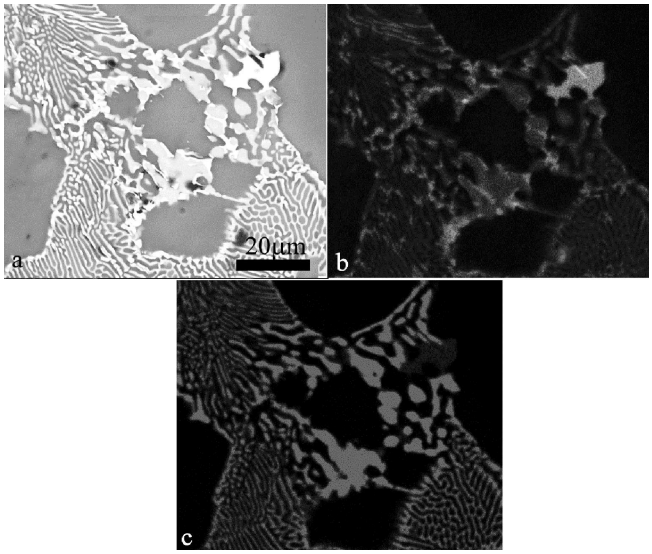

Fig. 5. As in Fig. 4, but for Mg10Ca20Gd.

A typical SEM EDX map recorded from Mg10Ca20Gd alloy cooled at 50 K min^{-1} is shown in Fig. 5. The elemental maps show clearly the presence of two different intermetallic phases. The first phase is similar to that observed in the Mg10Ca10Gd alloy with some Gd soluble in the Ca rich intermetallic phase. The second intermetallic phase is enriched with Gd but there is some Ca dissolution within this intermetallic phase. At a slower cooling rate of 5 K min^{-1} microstructure observed for the Mg10Ca20Gd is similar to that presented here.

4. Discussion

The HEXRD line profiles show only the presence of one intermetallic phase in the Mg10Ca5Gd and Mg10Ca10Gd alloys during solidification even though the Scheil solidification calculations predict the presence of two different intermetallic phases, namely Mg_2Ca and Mg_5Gd phases. The presence of only one intermetallic phase is also supported by the SEM analysis conducted on the as-solidified samples. There are, however, two intermetallic phases observed in the Mg10Ca20Gd alloys at both cooling rates as predicted with Scheil calculations. The diffraction patterns show that the intermetallic phases observed in Mg10Ca20Gd alloy are Mg_2Ca and Mg_5Gd phases.

The start of phase transformation temperatures predicted by the Scheil calculations are compared to those

measured with HEXRD and generally the temperatures at which α-Mg phase solidifies are higher from the HEXRD measurement as compared with the values predicted by Scheil calculations, Table II and Table III. The temperature predicted by Scheil calculations for the α-Mg phase was 60–80 °C lower than that measured with HEXRD for a cooling rate of 5 K min^{-1}. However, the formation temperature for the Mg_2Ca phase occurs in the temperature range 515–504 °C which is comparable with the predicted formation temperature for Mg_2Ca phase at 513–510 °C for the alloys investigated at a cooling rate of 5 K min^{-1}. The formation temperature of 504 °C observed for Mg_5Gd in Mg10Ca20Gd alloy was comparable with that predicted for Mg_5Gd with the Scheil calculations at 509 °C.

The increase in the cooling rate to 50 K min^{-1} did not suppress the temperature at which α-Mg phase was first observed, but the temperature at which Mg_2Ca formed was supressed to ≈450 °C for Mg10Ca5Gd and Mg10Ca20Gd alloys but the suppression was not significant for Mg10Ca10Gd alloy at ≈498 °C, Table III. This is a suppression of ≈50 °C from that predicted with the Scheil calculations. The Mg_5Gd phase formed at 417 °C for Mg10Ca20Gd alloy at a cooling rate of 50 K min^{-1} and is ≈90 °C suppression from that predicted with Scheil calculations.

The ternary phase diagram of the MgCaGd system is yet to be fully evaluated and some preliminary work was conducted by Fei et al. at 400 °C [9] on the Mg rich end of the phase diagram. In the current investigation the ternary phase reported by Fei et al. in their investigations was not observed. Additionally Mg_3Gd phase observed by Ding et al. [12] during their investigations of Mg1CaxGd alloys (x = 1–3 $wt\%$) was not observed in the current investigation. The Scheil calculations used for the current investigation were predicted by the extension of the three binary systems into the ternary phase field. Thus accurate measurements on the ternary solubilities and the extensions of phases due to solubility of Gd and Mg_2Ca and Ca and Mg_5Gd phases cannot be accurately predicted. Based on the current solidification studies it is envisaged that the Mg_2Ca phase has a larger solubility of Gd and extends into the ternary phase field more than the Mg_5Gd phase. It is not clear whether this extension is caused by the solubility differences between the two alloying additions in Mg. Gd has a wide solubility range with maximum solid solubility close to 23 wt%Gd [8] while Ca only has a maximum solid-solubility of 1.34 wt% in Mg [8]. The content of Gd in the alloys investigated is below the solubility limit of Gd and thus in case of 5 and 10Gd containing alloys the majority of Gd remains in solution both in Mg_2Ca intermetallic and the α-Mg matrix. However, there is a super-saturation of Gd in Mg10Ca20Gd alloy which causes Mg_5Gd phase to form.

5. Conclusions

In situ investigation of solidification of Mg10CaxGd (x = 5, 10, 20) showed that the change in cooling rate from 5 to 50 K min^{-1} did not result in changes of the type of intermetallic phases given the composition of the alloy. When the Gd content was less that 20 wt% only one intermetallic phase was observed and it was found to be Mg_2Ca phase. In Mg10Ca20Gd alloy, Mg_5Gd phase was observed in addition to the Mg_2Ca phase. The transformation start temperature for α-Mg phase predicted via the Scheil solidification calculations was lower than that observed during solidification while the transformation temperature for Mg_2Ca and Mg_5Gd phases observed with a cooling rate of 5 K min^{-1} was similar to those predicted by the Scheil calculations. However, the increase in the cooling rate to 50 K min^{-1} resulted in transformation start temperatures for observing Mg_2Ca and Mg_5Gd phases to lower temperatures than those predicted by the Scheil calculations.

Acknowledgments

The authors acknowledge the Deutsches Elektronen-Synchrotron for the provision of synchrotron radiation facilities in the framework of the proposal I-20130434I-20120627.

References

[1] N. Hort, Y. Huang, D. Fechner, M. Störmer, C. Blawert, F. Witte, C. Vogt, H. Drücker, R. Willumeit, K.U. Kainer, F. Feyerabend, *Acta Biomater.* **6**, 1714 (2010).

[2] L. Yang, Y. Huang, F. Feyerabend, R. Willumeit, C. Mendis, K.U. Kainer, N. Hort, *Acta Biomater.* **9**, 8499 (2013).

[3] M. Yamasaki, T. Anan, S. Yoshimoto, Y. Kawamura, *Scr. Mater.* **53**, 799 (2005).

[4] H. Yokobayashi, K. Kishida, H. Inui, M. Yamasaki, Y. Kawamura, *Acta Mater.* **59**, 7287 (2011).

[5] J.F. Nie, X. Gao, S.M. Zhu, *Scr. Mater.* **53**, 1049 (2005).

[6] K. Yamada, H. Hoshikawa, S. Maki, T. Ozaki, Y. Kuroki, S. Kamado, Y. Kojima, *Scr. Mater.* **61**, 636 (2009).

[7] T. Laser, Ch. Hartig, M.R. Nürnberg, D. Letzig, R. Bormann, *Acta Mater.* **56**, 2791 (2008).

[8] A.A. Nayeb-Hashemi, J.B. Clark, *Phase Diagrams of Binary Magnesium Alloys*, ASM International, Metal Park 1988.

[9] H.-J. Fei, G.-J. Xu, L.-B. Liu, H. Bo, L.-J. Zeng, C.-P. Chen, *Trans. Nonferrous Met. Soc. China* **23**, 881 (2013).

[10] S.M. He, X. Zeng, L. Peng, X. Guo, J. Chang, W. Ding, *Mater. Sci. Forum* **546–549**, 101 (2007).

[11] *Pearson's — Crystal Structure Database for Inorganic Compounds (on CD-ROM)*, Eds. P. Villars, K. Cenzual, Release 2012/13.

[12] Y.-T. Ding, Z. Zhao, D.-X. Liu, Y. Hu, *Lanzhou Ligong Daxue Xuebao* **39**, 1 (2013).